







Article

Multi-Response Optimization of Additively Manufactured Ti6Al4V Component Using Grey Relational Analysis Coupled with Entropy Weights

Khaled N. Alqahtani ¹, Abdulmajeed Dabwan ^{1,*}, Emad Hashiem Abualsauod ¹, Saqib Anwar ²,
Ali M. Al-Samhan ² and Husam Kaid ¹

¹ Industrial Engineering Department, College of Engineering, Taibah University, Medinah 41411, Saudi Arabia

² Industrial Engineering Department, College of Engineering, King Saud University, P.O. Box 800, Riyadh 11421, Saudi Arabia

* Correspondence: adabwan@taibahu.edu.sa

Abstract: Due to its near-net-shape manufacturing and ability to treat challenging-to-manufacture materials such as titanium alloys, Additive manufacturing (AM) is growing in popularity. However, due to the poor surface quality of AM components, finishing processes such as machining are required. One of the most difficult aspects of finishing AM components is the fact that even when using the same machining parameters, the surface roughness can vary significantly depending on the orientation of the part. In this study, electron beam melting (EBM) Ti6Al4V parts are subjected to the finishing (milling) process in three potential orientations relative to the direction of the tool feed. The impact of the feed rate, radial depth of cut, and cutting speed on the surface roughness and cutting force of the Ti6Al4V EBM part is studied while taking the orientations of the EBM components into consideration. It is found that the machined surface changes in noticeable ways with respect to orientation. A factorial design is used for the experiments, and analysis of variance (ANOVA) is used to evaluate the results. Furthermore, the grey relational analysis (GRA) method coupled with entropy weights is utilized to determine the optimal process variables for machining a Ti6Al4V EBM component. The results show that the feed rate has the greatest impact on the multi-response optimization, followed by the cutting speed, faces, and radial depth of cut.

Keywords: electron beam melting (EBM); surface roughness; Ti6Al4V; cutting force; part orientations; grey relational analysis (GRA); multi-response optimization



Citation: Alqahtani, K.N.; Dabwan, A.; Abualsauod, E.H.; Anwar, S.; Al-Samhan, A.M.; Kaid, H. Multi-Response Optimization of Additively Manufactured Ti6Al4V Component Using Grey Relational Analysis Coupled with Entropy Weights. *Metals* **2023**, *13*, 1130. <https://doi.org/10.3390/met13061130>

Academic Editors: Michela Simoncini and Tommaso Mancia

Received: 1 May 2023

Revised: 28 May 2023

Accepted: 14 June 2023

Published: 16 June 2023



Copyright: © 2023 by the authors. Licensee MDPI, Basel, Switzerland. This article is an open access article distributed under the terms and conditions of the Creative Commons Attribution (CC BY) license (<https://creativecommons.org/licenses/by/4.0/>).

1. Introduction

Ti6Al4V is the most extensively researched member of the family of lightweight alloys. Since the introduction of additive manufacturing (AM) techniques, titanium alloys have attracted considerable interest. Due to the advantages of additive manufacturing, its mechanical performance, and its corrosion resistance, it has found numerous applications [1]. The Ti6Al4V alloy is characterized by its high strength, low density, and high fracture toughness. Approximately 50% of all material markets recognize this alloy as the most prevalent titanium alloy. Initially, it was employed in the aircraft industry to construct intelligent aviation components. Due to the alloy's high strength-to-weight ratio, jet engines, gas turbines, and a variety of aircraft components can all benefit from the weight reductions this material provides. In addition, its high biocompatibility with the human body has led to a variety of biomedical applications [2]. Osseointegration, corrosion protection, and specific strength all contribute to Ti6Al4V's prominence as a medical-grade metal alloy [3,4]. However, it has a poor propensity to be machined [4], particularly when made through additive manufacturing (AM), due to its unusual microstructure, which is a function of the AM process parameters. Therefore, it is crucial to choose the appropriate cutting parameters to simultaneously decrease the cutting force and the surface roughness.

Additive manufacturing (AM) technologies provide a versatile, effective, and quick method for making complicated and individualized products [5]. One of the important techniques in AM is electron beam melting (EBM). EBM refers to a family of manufacturing methods in which materials are directly joined to create parts, typically in a layer-upon-layer fashion using 3D modeling data. The manufacturing of end-use parts with EBM is becoming increasingly common in the industry, which is hastening the development of related design, process, and manufacturing methods [6]. With the highly praised benefits of quick design-to-part transition and increased design freedoms, EBM methods continue to advance toward production-ready technologies [7]. EBM is positioned to bring about a revolution due to its innovative production model. It provides the possibility of bulk customization, flexible production, on-demand manufacturing, and decentralized production. Nonetheless, not only the complexity of manufacturing systems but also the desire for increasingly complex and high-quality products present several difficulties [8]. Poor surface quality and insufficient mechanical characteristics are also major problems for EBM processes [9].

In order to accomplish the desired material properties, tolerances, and surface finish in EBM production cycles, post-processing stages such as heat treatment and machining are often required [5]. Numerous investigations have been conducted to enhance the machinability of titanium alloy during the milling process; Iquebal et al. [10] presented the effects of Ti6Al4V EBM through machining and fine abrasive polishing. The results indicated that average surface roughness improved by 98.1% and surface hardness by 37.0%. In the case of abrasive finishing, the microhardness increased by 11% while the average surface roughness decreased by 99.82%. Gong et al. [11] demonstrated statistically significant differences in the machining behavior of Ti6Al4V across build directions in EBM specimens, as-AM, and after heat-treated laser powder bed fusion (L-PBF) specimens (21% reduced specific cutting power in L-PBF). Hojati et al. [12] studied the differences between micro-milling titanium alloy produced by selective laser melting (SLM), EBM, and conventional titanium. They tested the impact of various feeds per tooth on the surface roughness, cutting force, and burr formation. They discovered that despite EBM titanium's greater hardness, it produced the same or lower forces. Bonaiti et al. [13] investigated the micro-milling machinability of additively manufactured Ti6Al4V by analyzing surface roughness, cutting forces, and burr formation. Comparing the AM material to the conventional titanium alloy, they discovered several differences: due to a finer microstructure, AM material exhibited higher hardness; standard titanium exhibited greater surface roughness than AM titanium; despite exhibiting increased hardness, AM titanium exhibited lower cutting forces; and standard titanium exhibited superior results when considering burr formation. Rysava and Bruschi [14] compared the micro-milling characteristics of EBM and direct metal laser sintering (DMLS) Ti6Al4V alloys based on the influence of burr formation, surface topography, surface defects, roughness, tool damage, and microstructural modifications. The results demonstrated that the most crucial cutting parameter is the feed per tooth, which directly affects the final surface roughness, the formation of burrs, and the occurrence of surface defects. In addition, they observed adhered material on the tool edges as opposed to abrasion wear and no microstructural changes. Çevik et al. [15] enhanced the surface quality of samples made from Ti6Al4V alloy using powder bed-fed additive manufacturing with various processing parameters by applying an additional process, such as CNC machining. The Ti6Al4V samples exhibited greater machinability with lower cutting forces and lower surface roughness due to the material's rapid cooling. Yadav and Pawade [16] evaluated the compatibility and property variations of Ti6Al4V produced using AM methods (e.g., EBM, SLM, and direct energy deposition (DED)) to those produced via traditional manufacturing. According to the findings, the feed rate and the depth of cut are the most important factors in determining the presence and severity of defects (such as shallow grooves, micro-particle deposits, white layers, etc.) on the turned surfaces of Ti6Al4V alloy. SLM and DED both have almost 20% greater ultimate tensile strength and yield strength than EBM. Sartori et al. [17] investigated the turning of Ti6Al4V

components manufactured by EBM and DMLS. When compared to EBM and wrought material, the DMLS-induced added characteristics demonstrated higher hardness and lower thermal conductivity. Because of this variation, spinning DMLS in dry conditions produced the deepest crater in the tool.

Some studies have shown that the 3D printing layer orientations have a substantial impact on the final appearance of the additively made components. For example, the impact of the layers' orientations during EBM milling and turning of Ti6Al4V components and milling γ -TiAl components was investigated by [18–20]. The researchers discovered that different EBM component orientations during machining can result in different levels of surface roughness, even when using the same machining settings. The part orientation impact was mitigated for EBM Ti6Al4V components through heat treatment [21]. Another study [22] looked into how adjusting the layer thickness in L-PBF fabrication of stainless steel 316L parts affected milling orientations. Cozzolino et al. [23] studied the energy required to manufacture a Ti6Al4V EBM part and then turned it to achieve the desired surface roughness. The results indicate that all samples have a high surface roughness, with Ra values ranging from 27.09 to 37.95 μm in the parallel direction and from 15.66 to 34.00 μm in the perpendicular direction. After the turning process, the direction parallel to the axis of the cylindrical samples has roughness values greater than in the direction perpendicular to the axis. Moreover, Cozzolino and Astarita [24] studied the influence of the milling process parameters of EBM Ti6Al4V components in order to improve surface finishing and energy consumption. The results show that the roughness varies along the parallel direction more than the perpendicular direction due to the face. The best surface roughness is achieved by using a spindle speed of 1600 RPM and a depth of cut of 0.3 mm. Instead, although it results in somewhat higher roughness than the other process settings, the medium spindle speed (2500 rev/min) and the highest depth of cut (0.9 mm) of our experimental campaign should be chosen if minimizing overall energy consumption is the main target. While the impact of layer orientation on finishing the EBM part is known to be important, no report has been discovered to date that optimizes this effect.

Grey relational analysis (GRA) with entropy weights can solve multi-response optimization problems involving multiple criteria, and its use in multi-response problems has acquired popularity [25–27]. Dabwan et al. [28] applied the grey relational method with entropy weights to identify the optimal process parameters for single-point incremental forming products and found that the tool diameter has the greatest effect on the thinning of the single-point incremental forming process. She et al. [29] optimized the bending performance of optical fibers by employing grey relational analysis and discovered that the bending loss decreased by an order of magnitude. Chen et al. [30] optimized the door panel design for automobiles using Grey relational analysis and entropy weight. The results demonstrate that the optimized structure reduces the door's weight and that the door's performance meets the minimum requirements. It is still possible to use multi-response discrete optimization in various studies and to integrate it into manufacturing processes.

Results from various studies indicate that it is not feasible to predict how EBM processes will affect the machinability of the material and that each EBM process will have its own unique impact on the additively produced components. Therefore, more effort must be devoted to determining the impact of various EBM techniques on the machinability of the materials. The different part orientations are one of the important factors influencing EBM methods of machinability. Milling AM components while considering part orientations is difficult, but only a few studies have been devoted to tackling this issue. The purpose of this study is to analyze the effects of milling EBM Ti6Al4V components at different part orientations, feed rates, radial depths of cut, and cutting speeds on surface roughness and cutting forces, as shown in Figure 1. Furthermore, the influence of the EBM process on the machinability of Ti6Al4V is optimized using grey relational analysis coupled with entropy weights to improve the machined surface of the Ti6Al4V EBM part.

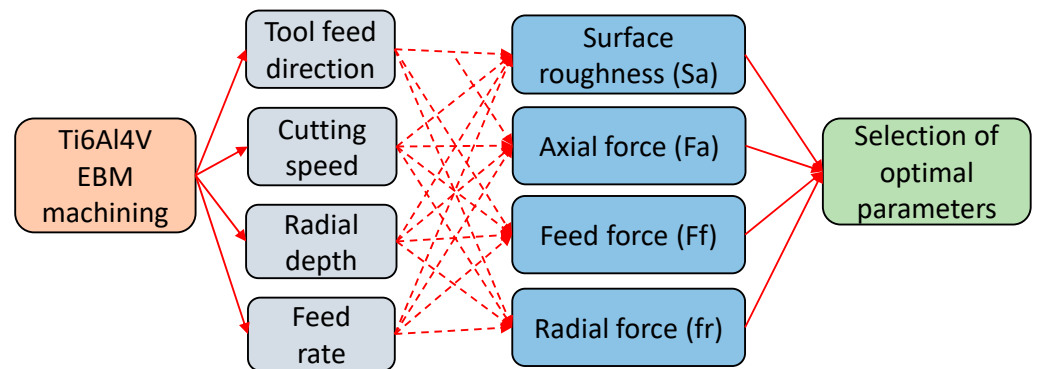


Figure 1. Marking diagram for the selection of EBM Ti6Al4V milling process parameters.

2. Materials and Methods

2.1. Material Details

Samples of Ti6Al4V were manufactured using the ARCAM EBM technique and measured 30 mm on a side, 30 mm in height, and 10 mm in depth (see Figure 2). The average particle size of the Ti6Al4V powder is 71 μm . Table 1 lists the components that compose the powdered form of Ti6Al4V. The primary EBM process parameters utilized in the fabrication of the Ti6Al4V components are listed in Table 2. The EBM variables in Table 2 were chosen based on past research, suggesting that these values were indicated by ARCAM as the default for achieving desirable microstructures and mechanical characteristics [31,32].

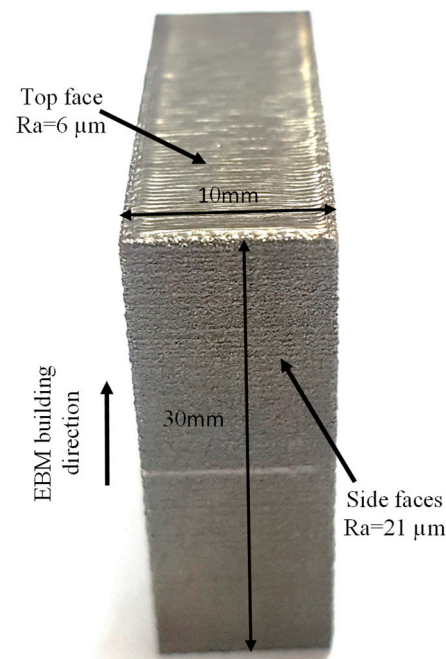


Figure 2. A three-dimensional component manufactured by electron beam melting (EBM).

Table 1. Composition of Ti6Al4V powder data from [33].

Elements	Aluminum	Vanadium	Carbon	Iron	Oxygen	Titanium
Percentage (wt.%)	6.04	4.05	0.013	0.0107	0.13	Balanced

Table 2. Parameters of the EBM for Ti6Al4V parts data from [31,32].

EBM Parameters	Values
Solidus temperature	1878 K
Focus offset	3 mA
Acceleration voltage	60 kV
Preheat temperature	750 °C
Powder layer thickness	0.05 mm
Scan speed	4530 mm/s
Electron beam diameter	200 µm
Liquidus temperature	1928 K
Line offset	0.1 Mm
Beam current	15 mA

2.2. Milling Options and Measurements Setups

The faces of EBM-manufactured components have varying surface qualities. For instance, the upper surfaces of EBM Ti6Al4V components have a Sa value of 6 µm, while the side surfaces have a Sa value of 21 µm. Despite the fact that EBM components were manufactured using the optimized parameters discovered in prior research [32], the average surface roughness value on the side surfaces is still Sa = 21 µm, which is inadequate for many applications. The top and side surface roughnesses were found to be about the same (Sa = 7.5 µm and Sa = 21 µm, respectively) after employing the optimized scan methods, as reported by [34]. Therefore, an additional operation must be performed on the EBM components in order to produce a smooth surface. In this research, the conventional vertical milling method is employed for the secondary operation.

For the best possible surface finish when machining EBM components, it is essential to have the 3D-printed part oriented in the optimal fashion with regard to the tool feed direction (TFD). When milling an EBM component, the tool can be fed in one of three directions: (1) perpendicular to the layer planes (Direction 1), (2) parallel to the layer planes (Direction 2), or (3) in the layer plane itself (Direction 3). The orientations of these three parts with regard to the TFD are depicted schematically in Figure 3. The first direction is called “tool movement perpendicular to layer planes”, and it occurs when the TFD is orthogonal to the layer planes (Direction 1). The second orientation is called “tool moving parallel to layers planes”, and it occurs when the TFD is aligned to the planes of the layers being worked on (Direction 2). In the third configuration, known as “tool movement in a layer plane”, the feed path of the tool lies in the same plane as an EBM layer (Direction 3).

The milling setup is depicted in Figure 4a, and the three tool feed orientations (Direction 1, Direction 2, and Direction 3) are shown in Figure 4b for an EBM component. The samples were machined with a 30 mm/min feed rate, 10 mm tool diameter, 50 m/min cutting speed, and 0.4 mm depth of cut to smooth them out before the real experiments were performed. This was done to smooth out the rough and irregular EBM-created surfaces so they could be machined more easily. To evaluate the impact of EBM part orientation on milling quality, milling was carried out using the process settings shown in Table 3. Table 3 shows process values that are consistent with those found in prior research on machining Ti6Al4V [35–37].

Table 3. Milling process parameters.

Process Parameters	Values
Tool feed direction, (TFD)	Direction 1, Direction 2, Direction 3
Cutting speed, (V) m/min	50, 80
Radial depth of cut, (Rd) mm	2.4, 4.8
Depth of cut, (d) mm	0.4
Feed rate, (f) mm/min	30, 60

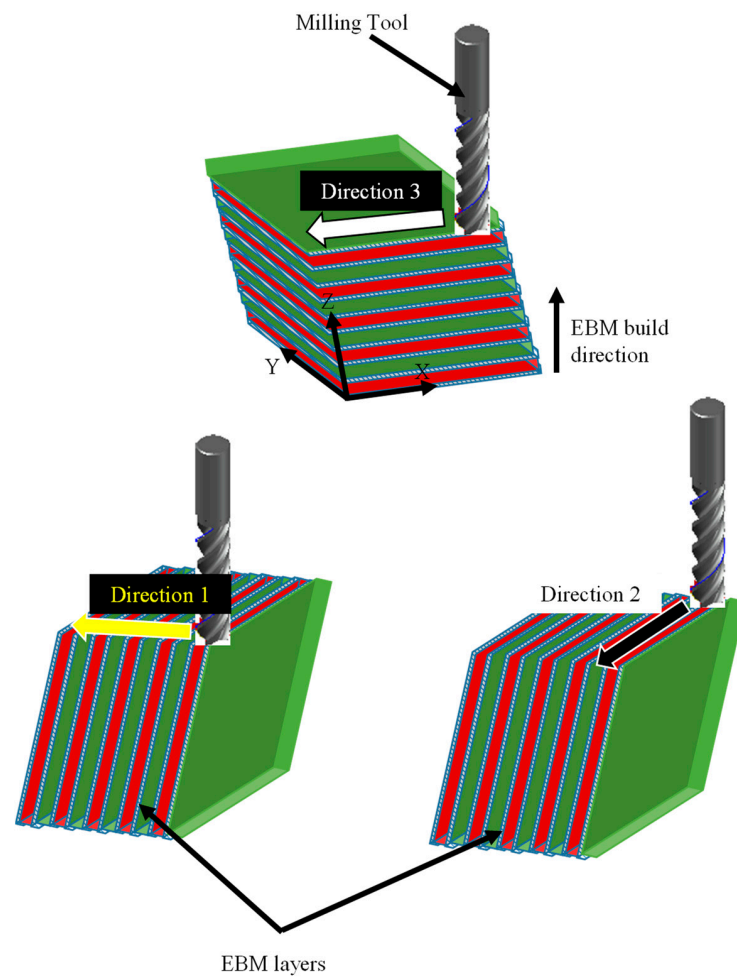


Figure 3. A schematic depiction of milling direction choices for EBM parts.

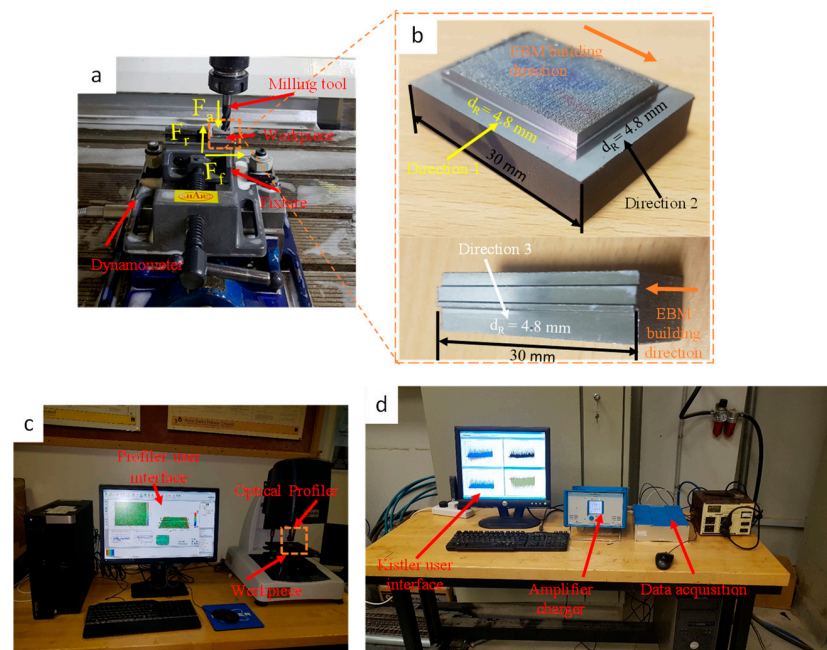


Figure 4. (a) Machining process setup of the EBM-manufactured component; (b) A magnified image of a machined component, showing its orientations, with labels; (c) 3D optical profilometer setup; (d) dynamometer.

DMG Mori's (Oelde, Germany) DMC 635 V Ecoline vertical milling machine was used for the milling operations. 24 m/min of maximum feed rate, 1 μm of positioning accuracy, and 8000 rpm of maximum spindle speed are the specifications of this milling machine. The tool code is ISO: 1P240-1000-XA 1630 and material Id: 6259717, with a four-fluted 10 mm diameter solid carbide end mill tool having a length of 72 mm, a radial rake angle of 9° , an axial rake angle of 5.5° , and a flute helix angle of 35° from SANDVIK COROMANT. The cutting forces and the surface roughness were the two responses evaluated. Sa is a surface roughness parameter that was used to measure the degree of roughness across all three directions. The surface roughness (Sa) of the milled components was measured using a Bruker (Berlin, Germany) Contour GT-K 3D optical profilometer. ISO 25178-2 was used as the standard for filtration. After milling, the machined surface was scanned at 3 mm intervals in five distinct locations along each of the three directions (Direction 1, Direction 2, and Direction 3). The Sa was measured by measuring a 2.2 mm by 1.7 mm area at each reading, and the meaning of the five readings for each orientation was recorded. As shown in Figure 4c, during milling, the axial force (Fa), feed force (Ff), and radial force (Fr) were measured by placing the component in a fixture and then using a Kistler 5697A piezoelectric dynamometer (Kistler Instrument AG, Winterthur, Switzerland), as shown in Figure 4d. The frequency of force data sampling was 1000 Hertz. The surface morphology of the components was evaluated after the milling process using a scanning electron microscope (SEM) manufactured by Jeol, Tokyo, Japan (Model JCM 6000Plus).

2.3. Grey Relational Analysis (GRA) with Entropy Weights

This study also employs a GRA-based optimization strategy in conjunction with entropy weights to determine the optimal combination of process parameters for the machined EBM Ti6Al4V part [28,38]. GRA is one of the most intelligent decision-making methods in an industrial context; it relies on original data; provides quick and straightforward estimates; and requires minimal training or expertise to implement [39,40]. Furthermore, it has a small data size and can be effectively applied in multi-factor evaluation. The GRA strategy is exemplified below [41–43]. Linear normalization is a data transformation performed by GRA to make otherwise incomparable input data fall within the range of 0 to 1. Equations (1) through (3) represent the normalized information for the i th experiment and the k th response (or quality measure).

$$x_i^*(k) = \frac{x_i^{(O)}(k) - \min x_i^{(O)}(k)}{\max x_i^{(O)}(k) - \min x_i^{(O)}(k)} \text{ Higher-the-better} \quad (1)$$

$$x_i^*(k) = \frac{\max x_i^{(O)}(k) - x_i^{(O)}(k)}{\max x_i^{(O)}(k) - \min x_i^{(O)}(k)} \text{ Lower-the-better} \quad (2)$$

$$x_i^*(k) = \frac{|x_i^{(O)}(k) - TV|}{\max\{\max x_i^{(O)}(k) - TV, TV - \min x_i^{(O)}(k)\}} \text{ Nominal-the-better (TV=Target Value)} \quad (3)$$

Consequently, a reference sequence is determined using standardized (or comparability) sequences. The Grey Relational Coefficient (GRC) is computed by putting the normalized sequences into Equation (4).

$$\text{GRC} (x_o^*(k), x_i^*(k)) = \frac{\Delta_{\min} + \epsilon \Delta_{\max}}{\Delta_{oi}(k) + \epsilon \Delta_{\max}} \quad (4)$$

where

$\Delta_{oi}(k)$ represents the differences between a sequence of normal (x_i^*). Furthermore, a sequence of references (x_o^*) is denoted by the symbolization $o_i(k)$, where $x_o^*(k)$, is the sequence of standard and $x_i^*(k)$ the sequence between the sequence of reference $x_o^*(k)$, and

the normalized sequence $x_i^*(k)$, i.e., $\Delta_{oi}(k) = |x_o^*(k) - x_i^*(k)|$ is the absolute value of the difference between $x_o^*(k)$ and $x_i^*(k)$.

$\Delta_{min} = \min_{\forall i} \min_{\forall k} \Delta_{oi}(k)$ and $\Delta_{max} = \max_{\forall i} \max_{\forall k} \Delta_{oi}(k)$, where $i = 1, 2, \dots, m$ and $k = 1, 2, \dots, n$.
 ε : distinguishing coefficient, $\varepsilon \in [0, 1]$.

Individual GRCs are grouped into a singular multi-response parameter during the subsequent phase. This is accomplished by assigning weights to each GRC and subsequently combining them. Individual GRC response weighting variables are analyzed using the entropy method [43]. Entropy weight calculation is a method for objectively evaluating the relative weights of responses based on their inherent information. As a result, disturbance can be reduced in the resulting weights, leading to impartial results [43,44]. This method depends on the number of data and thus reveals effective response information. The response's larger entropy weight indicates its higher significance. Assume there are n responses and m experiments, whereas x_{ij} represents the value of i th experiment and j th response. It is possible to make a rough approximation of the entropy weight using Equations (5)–(8) [43,44].

Adjusting numbers for the i th experiment and the j th response so that they are normalized, r_{ij}

$$\text{Response of benefit (higher the better)} = \frac{x_{ij}}{x_{max}} \quad (5)$$

$$\text{Response of cost (smaller the better)} = \frac{x_{min}}{x_{ij}} \quad (6)$$

where, $(i = 1, 2, 3, 4, \dots, m; j = 1, 2, 3, \dots, n)$

Entropy computation

$$H_j = - \frac{\sum_{i=1}^m P_{ij} \ln P_{ij}}{\ln m} \quad (i = 1, 2, 3, 4, \dots, m; j = 1, 2, 3, \dots, n) \quad (7)$$

where, $P_{ij} = \frac{r_{ij}}{\sum_{i=1}^m r_{ij}}$ ($i = 1, 2, 3, 4, \dots, m; j = 1, 2, 3, \dots, n$)

Estimation of the weight of entropy

$$w_j = \frac{1 - H_j}{n - \sum_{j=1}^n H_j}, \quad \sum_{j=1}^n w_j = 1, \quad (j = 1, 2, 3, \dots, n) \quad (8)$$

Grey relational grade (GRG) is a metric that incorporates weighting with the proper GRC in each experiment. The GRG is used to evaluate the overall performance of multi-response optimization.

$$\text{GRGi} = \sum_{k=1}^n w_k \text{GRCik} \quad (9)$$

where GRGi represents the GRG for i th experiment, w_k represents the weighting for the k th response, and n represents the response number. From a design of m experiments (in the present study, forty-eight), the combination of experiments with the largest GRG presents the best multi-response performance, i.e., the experiment with the largest GRG results in the process parameter configuration that generates the optimal performance.

3. Results and Discussion

The measurements and design of experiments (DOE) matrices with two replications are listed in random sequence in Table A1.

3.1. ANOVA Analysis

Analysis of variance (ANOVA) was utilized to examine the significant factors and interactions for each response. Reducing the model by removing nonsignificant ($p < 0.05$) variables one by one unless they are part of a significant higher-level interaction. The term with the highest p value is eliminated first, and the procedure of fitting is repeated. The ANOVA is run again, and the elimination procedure is repeated until a reduced model

containing all significant terms is obtained. Table A2 presents the reduced model of an analysis of variance (ANOVA) for surface roughness (Sa), which reveals that the variables Face, cutting speed (V), feed rate (f), and radial depth of cut (Rd) have a significant effect on the output, which are consistent with those found by [19,21]. There is a considerable effect on the Sa from two-source interactions such the Face and V, Face and f, Face and Rd, V and f, and V and Rd. Moreover, three-source interactions, including Face, V, and f, Face, V, and Rd, and Face, f, and Rd, have significant effects on the Sa. The R-square, adjusted R-square, and predicted R-square values presented in Table A2 indicate that the model terms provide an outstanding representation of the data variability.

Table A3 displays the findings of an ANOVA for radial force (Fr), which reveals that the variables Face, Feed rate (f), and Radial depth of cut (Rd) have a significant effect on output, as reported by [19]. There is a significant effect on the Sa from two-source interactions such the Face and f, V and f, and f, and Rd. Moreover, three-source interactions, including V, f, and Rd have significant effects on the Sa. The R-square, adjusted R-square, and predicted R-square values presented in Table A3 indicate that the model terms provide an outstanding representation of the data variability.

The ANOVA results for Feed force (Ff) presented in Table A4 indicate that Feed rate (f) and Radial depth of cut (Rd) have a significant effect on output. Only one significant effect on the Sa from two-source interactions including V and f was found. Moreover, three-source interactions, including Face, V, and F and V, f and Rd have significant effects on the Sa. The R-square, adjusted R-square, and predicted R-square values presented in Table A4 indicate that the model terms provide an outstanding representation of the data variability.

Table A5's ANOVA results for Axial force (Fa) indicate that Cutting speed (V) and Feed rate (f) have a significant effect on output, as reported by [45]. There is a significant effect on the Sa from two-source interactions such the V and Rd, and f and Rd. Moreover, three-source interactions, including Face, V, and f and V, f, and Rd have significant effects on the Sa. The R-square, adjusted R-square, and predicted R-square values presented in Table A5 indicate that the model terms provide an outstanding representation of the data variability.

3.2. Grey Relational Analysis (GRA) with Entropy Weights Analysis

As a first step in the GRA implementation, the experimental findings from Table A1 are normalized between 0 and 1 under the lower-the-better condition using Equation (2). Both the reference sequence $x_0^*(k)$ and the standardized or comparability sequence $x_i^*(k)$ (k) are given to response quantities. After cleaning the data, an overview of all sequences can be found in Table A6. As stated by Deng (1989) [46], a higher number of normalized values correlates with optimal performance and, consequently, shows greater efficacy.

The deviation sequences $\Delta_{01}(k)$ in Table A7, can be obtained as follows.

$$\Delta_{01}(1) = |x_0^*(1) - x_1^*(1)| = |1 - 0.5734| = 0.4266$$

$$\Delta_{01}(2) = |x_0^*(2) - x_1^*(2)| = |1 - 0.2320| = 0.7680$$

$$\Delta_{01}(3) = |x_0^*(3) - x_1^*(3)| = |1 - 0.2319| = 0.7681$$

$$\Delta_{01}(4) = |x_0^*(4) - x_1^*(4)| = |1 - 0.0503| = 0.9497$$

therefore, $\Delta_{01} = (0.4266, 0.7680, 0.7681, 0.9497)$.

Results for all Δ_{0i} for $i = 1, \dots, 48$ are shown in Table A7 and the same calculation method is used for $i = 2, 3, 4, \dots, 48$.

By analyzing the data in Table A8, Δ_{\min} (k) and Δ_{\max} (k) can be defined as follows.

$$\Delta_{\min} = \Delta_{021} (1) = \Delta_{021} (2) = \Delta_{032} (3) = 0.0000$$

$$\Delta_{\max} = \Delta_{026} (1) = \Delta_{018} (2) = \Delta_{018} (3) = 1.0000$$

Differentiating coefficient integration $\varepsilon = 0.5$ into Equation (6) yields the GRC for each response.

Listed below are examples of the GRC_i (k) approximation.

$$\text{GRC1} (1) = \frac{0.0000 + 0.5 \times (1.0000)}{0.4266 + 0.5 \times (1.0000)} = 0.5396$$

$$\text{GRC1} (2) = \frac{0.0000 + 0.5 \times (1.0000)}{0.7680 + 0.5 \times (1.0000)} = 0.3943$$

$$\text{GRC1} (3) = \frac{0.0000 + 0.5 \times (1.0000)}{0.7681 + 0.5 \times (1.0000)} = 0.3943$$

$$\text{GRC1} (4) = \frac{0.0000 + 0.5 \times (1.0000)}{0.9497 + 0.5 \times (1.0000)} = 0.3449$$

Hence, GRC1(k) = (0.5396, 0.3943, 0.3943, 0.3449), k = 1, 2, 3. The same steps are taken for $i = 2, 3, 4, \dots, 48$. Table A8 illustrates the GRC for every experiment conducted.

Weights for every measure of performance must be known in order to optimize a problem with numerous responses. Expertise and trial-and-error are highly reliant on the traditional method of evaluating the values of each response, leading to a rise in decision-making uncertainty. Entropy is introduced as a technique for dispassionately assessing the significance of each response in GRA. The GRC of each quality measure is represented by an element in Table A6 of the array Multiple Quality Characteristics (MQC). The estimated weights in Equations (4)–(7) are calculated using this data.

The GRG of the experiments' comparability sequence can be obtained as shown in Table A9.

Based on the experimental design, Table A9 reveals that the machining of Ti6Al4V experiment number 19 has the highest GRG. Consequently, experiment number 19 determines the optimal multi-response parameter from the 48 experiments.

The average GRG for each parameter level is calculated to identify the best set of processing variables for enhanced usefulness. This procedure clusters the GRGs based on the process parameter levels in each column, then averages the parameters with the same parameter levels. For example, for the factor faces (Table A1), experiments 1, 2, 3, 4, 5, 6, 7, 8, 25, 26, 27, 28, 29, 30, and 32 are adjusted to level 1. Consequently, the average GRG for A1 can be determined by analyzing the data in Table A10:

$$A1 = \frac{0.41828 + 0.56443 + 0.7633 + 0.58548 + \dots + 0.61729 + 0.64201 + 0.66599}{16} = \frac{9.612681073}{16} = 0.600793$$

Both A2 and A3 are predicted to have average GRGs of 0.56073 and 0.565408, respectively.

Each level of machining parameter is computed using the same procedure, and Table A10's main effect analysis is performed.

Figure 5 demonstrates that the various responses of the machining of the EBM Ti6Al4V component are influenced by changes to the process variables. The selection in faces (Direction 1) and decrease in radial depth of cut increases the GRGs, leading to a decrease in surface roughness and cutting forces which are consistent with [19–21]. However, as cutting speed and feed rate decrease from a greater to a lesser value, the relational grades for the output characteristics diminish. This indicates that increased cutting speed and feed rate are essential for minimizing surface roughness and cutting force. Changes from

level 1 to level 2 and level 3 in faces have a significant influence on surface roughness and cutting force. The surface morphology of milled Ti6Al4V EBM in three directions is shown in Figure 6. Scanning electron micrographs (SEM) reveal various tool feed marks. The prominent tool feed marks are generated when the milling tool is moved parallel to the layers' planes, which impart larger roughness on the surface after machining, as shown in Figure 6c. While the thick tool feed marks are generated when the interfaces between successive layers are perpendicular to the tool feed direction, leading to large surface roughness, as shown in Figure 6b. Furthermore, the minor tool feed marks are generated when the milling tool is moved perpendicular to the layers, which achieved a smaller surface roughness, as shown in Figure 6a. All of this is consistent with [19–22].

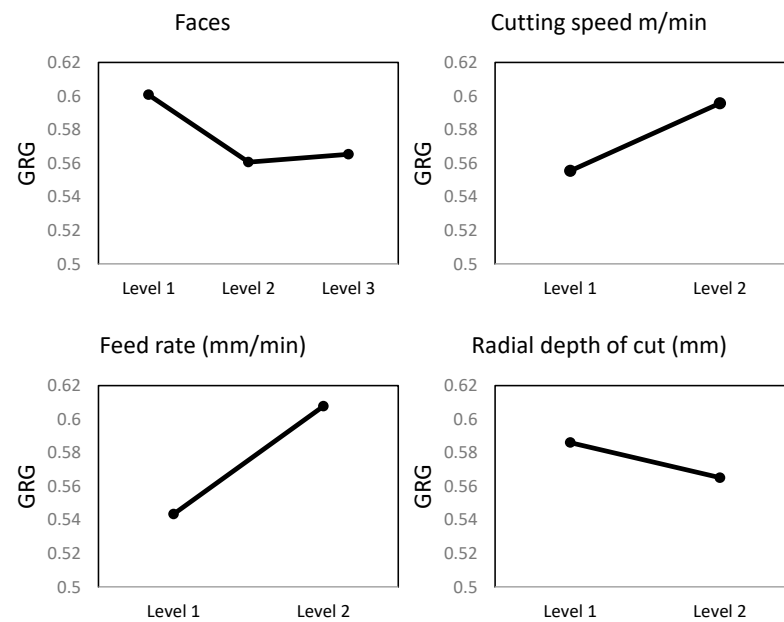


Figure 5. Influence of process variable levels on various quality attributes.

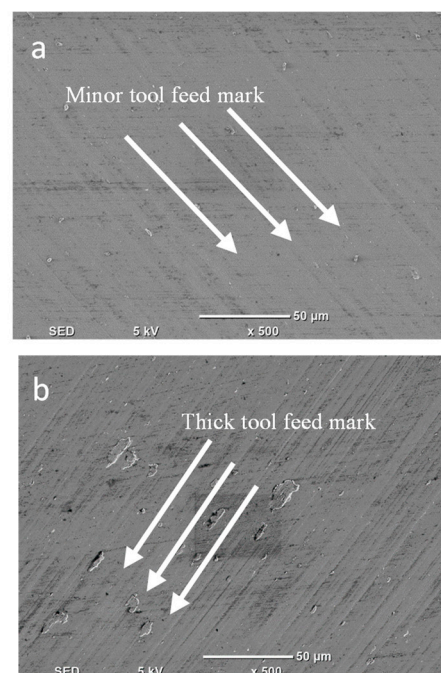


Figure 6. Cont.

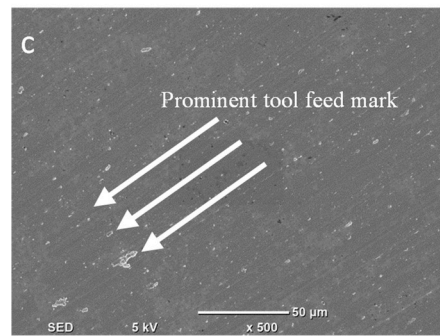


Figure 6. SEM image for the milled surface of EBM orientations: (a) Direction 1; (b) Direction 2; (c) Direction 3 at 80 m/min of cutting speed, 30 mm/min of feed rate, and 2.4 mm of radial depth.

The difference in surface roughness among the three directions is because the tool interacts with a single EBM layer while machining along Direction 3 and exerts compressive forces at the EBM layer interface, which causes the bonded layers to rupture, resulting in a high surface roughness. In contrast, if the tool is fed in Direction 1, it interacts/cuts the group of layers with radial depth while exerting force on the layer bonds/interfaces, thereby preventing the tearing of adjacent layers. The layer interfaces still experience tensile stresses when Direction 2 is employed, and bond breaking may take place as the tool is fed throughout the layer group. This contributes to Direction 2's mild roughness. Figure 7 shows the differences in 3D surface topography characterizations extracted along Direction 1, Direction 2, and Direction 3.

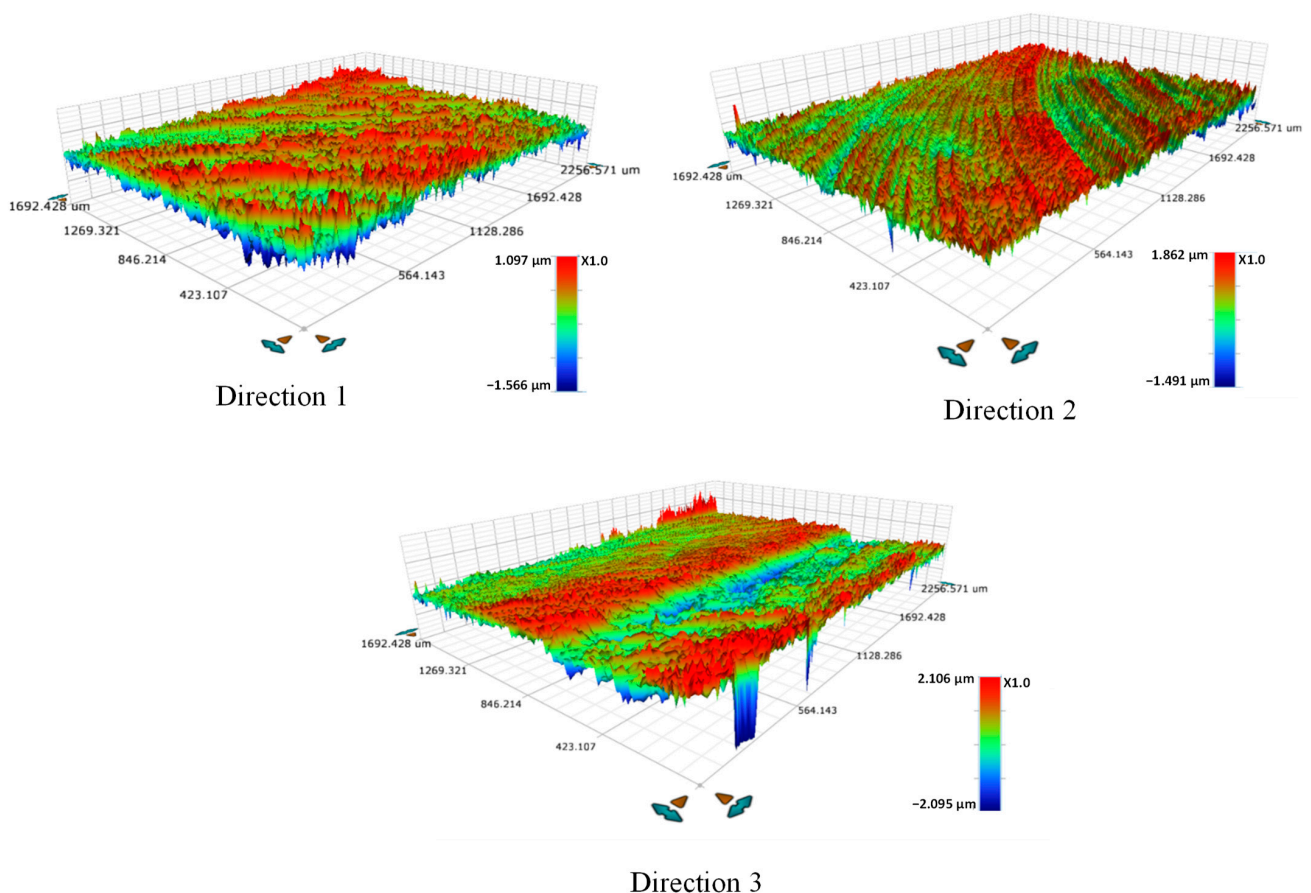


Figure 7. 3D surface topography characterizations at $V = 50$ m/min, $f = 30$ mm/min, and $Rd = 2.4$ mm for the three directions.

Regarding the cutting forces, when machining is conducted in Direction 1, the tool interacts with a group of EBM-bonded layers without causing tensile stresses at the interfaces of the layers. This results in different cutting forces in Direction 1 compared to Direction 3, in which the tool passes/cuts a single EBM layer while exerting maximal tensile forces on the interfaces, resulting in the lowest machining resistance. On the other hand, in Direction 2, the tool traverses multiple layers covered by the radial depth of cut. However, the interfaces of the layers are still subjected to tearing forces, which degrade the material for cutting, and intermediate cutting forces are generated. The results of surface morphology, roughness, and cutting forces are consistent with the result of GRG.

Therefore, by choosing the parameter level with the highest GRG (level 1 in faces, level 2 in cutting speed, level 1 in feed rate, and level 1 in the radial depth of cut; Figure 5), the optimal combination of process parameters can be easily derived from the main effect analysis. The optimal parameter settings that produce the lowest surface roughness and cutting force for machined EBM Ti6Al4V parts are predicted to be level 1 for faces, feed rate, and radial depth of cut, and level 2 for cutting speed.

The level-wise GRG (Figure 5) demonstrates the change in the multi-response as the process parameters progress from levels one to levels two and three. Comparing the values in the final column of Table A10, the difference between the minimum and maximum GRG values for factor feed rate is clearly the greatest, followed by factors cutting speed, faces, and radial depth of cut. This demonstrates that the feed rate has the greatest impact on multi-response optimization, followed by cutting speed, faces, and radial depth of cut.

4. Conclusions

This study demonstrates the value of careful process parameter control in the milling of Ti6Al4V components made through the EBM process. This study firmly establishes the significance and impact of controlling process factors on a finished machined surface. Improved surface roughness and less cutting force are two outcomes of this study's work on the Ti6Al4V EBM component. Furthermore, the effect of milling parameters on the part orientation of the Ti6Al4V EBM component is optimized using the grey relational analysis (GRA) technique with entropy weights.

The following are the main points of conclusion:

- Feed rate is the most important component when assessing surface roughness and cutting force regarding the milling process for the Ti6Al4V EBM part.
- Cutting speed is the second factor that affects the surface roughness and cutting force for the milling performance of the Ti6Al4V EBM part.
- The selection of the direction of layer orientation in the EBM part has a significant effect during the milling process to achieve minimum surface roughness and cutting force.
- The radial depth of cut is the lowest effect factor during the milling process for the Ti6Al4V EBM part.
- The study also concludes that the part orientation effect is likely one of the most important factors governing the surface roughness and surface morphology of the machined EBM Ti6Al4V component.
- The multi-response optimization (GRA-Entropy) shows that the optimal machining efficiency of a Ti6Al4V EBM component can be achieved if the component is machined in direction 1 at a feed rate of 60 mm/min, a cutting speed of 80 m/min, and a radial depth of cut of 2.4 mm.

Author Contributions: Conceptualization, A.D., S.A. and A.M.A.-S.; methodology, A.D. and H.K.; validation, A.D. and E.H.A.; formal analysis, A.D. and K.N.A.; investigation, A.D., S.A. and A.M.A.-S.; data curation, A.D., E.H.A., H.K. and K.N.A.; writing—original draft preparation, A.D.; writing—review and editing, S.A., A.M.A.-S., K.N.A. and E.H.A.; visualization, A.D.; supervision, S.A. and A.M.A.-S.; resources, K.N.A. and E.H.A. All authors have read and agreed to the published version of the manuscript.

Funding: Researchers Supporting Project number (RC442/50), Taibah University, Medinah, Saudi Arabia.

Data Availability Statement: All data generated or analyzed during this study are included in the present article.

Acknowledgments: The authors extend their appreciation to, Taibah University, represented by the Deanship of Scientific Research, for funding this project No. (RC-442/50).

Conflicts of Interest: The authors declare no conflict of interest.

Appendix A

Table A1. DOE matrix and corresponding results.

9	Input Parameters				Responses			
	Faces	V (m/min)	f (mm/min)	Rd (mm)	Sa (μm)	Fr (N)	Ff (N)	Fa (N)
1	C	50	30	2.4	0.145	147.1	73.02	177.3
2	B	50	30	2.4	0.193	102.8	99.63	173.2
3	A	50	30	2.4	0.147	90.04	88.6	171.5
4	A	50	30	2.4	0.148	114.1	78	170
5	A	80	30	4.8	0.114	31.68	85.46	154.6
6	A	80	30	4.8	0.116	41.66	82.59	152.6
7	B	50	60	2.4	0.142	6.21	46.12	152.6
8	C	50	30	2.4	0.144	139.3	60.23	149.1
9	B	50	60	4.8	0.156	65.78	72.51	138.7
10	A	80	60	4.8	0.146	20.03	74.06	137.9
11	C	80	60	4.8	0.127	65.65	54.63	126.1
12	B	80	30	4.8	0.136	49.29	80.35	123.5
13	C	50	30	4.8	0.177	56.11	55.17	119.7
14	B	80	60	4.8	0.157	20.71	61.41	119.4
15	B	80	30	4.8	0.137	9.75	77.08	118.3
16	B	80	30	2.4	0.175	64.2	49.17	117.9
17	B	80	60	2.4	0.159	64.2	49.17	117.9
18	B	50	60	2.4	0.131	9.07	48.81	117.6
19	C	50	30	4.8	0.186	49.7	55.07	117.2
20	C	80	30	2.4	0.178	65.95	48.88	109.2
21	C	50	60	4.8	0.179	61.02	45.88	106.6
22	C	50	60	4.8	0.182	58.09	45.18	106.4
23	C	80	30	4.8	0.152	47.22	48.9	104.4
24	C	80	60	4.8	0.14	7.916	45.1	103.9
25	B	50	60	4.8	0.154	58.64	50.47	103.8
26	B	50	30	4.8	0.154	21.41	45.55	102.4
27	A	50	30	4.8	0.173	34.23	53.66	102.3
28	B	50	30	2.4	0.189	60.07	50.63	102
29	A	50	60	4.8	0.157	11.22	52.14	101.2
30	A	50	60	4.8	0.165	15.07	50.53	99.89
31	A	50	30	4.8	0.165	29.55	46.04	94.71
32	C	80	60	2.4	0.152	54.25	67.95	88.59
33	A	80	60	2.4	0.164	50.5	53.77	76.64
34	B	50	30	4.8	0.146	38.76	41.43	74.52
35	C	80	60	2.4	0.154	35.9	57.44	74.49
36	C	80	30	4.8	0.151	41.23	39.11	73.74
37	A	50	60	2.4	0.135	11.72	14.84	72.74
38	A	50	60	2.4	0.132	22.38	27.66	71.54
39	B	80	60	2.4	0.16	49.21	36.93	71.49
40	A	80	60	4.8	0.136	44.01	26.2	67.06
41	A	80	30	2.4	0.127	75.45	39.58	61.4
42	A	80	60	2.4	0.161	29.58	40.61	50.86
43	B	80	30	2.4	0.165	13.33	21.93	46.41
44	A	80	30	2.4	0.127	24.6	27.19	43.66
45	B	80	60	4.8	0.157	37.62	19.27	43.14
46	C	80	30	2.4	0.175	56.98	16.39	36.98
47	C	50	60	2.4	0.191	6.755	6.378	32.22
48	C	50	60	2.4	0.188	4.895	11.07	31.37

Table A2. ANOVA results for Sa.

Source	DF	Seq SS	Adj SS	Adj MS	F-Value	p-Value
Model	20	0.01748	0.01748	0.000874	17.02	0
Face	2	0.003046	0.003046	0.001523	29.67	0
V	1	0.002023	0.002023	0.002023	39.4	0
f	1	0.000001	0.000001	0.000001	0.02	0.898
Rd	1	0.000295	0.000295	0.000295	5.74	0.024
Face*V	2	0.000713	0.000713	0.000356	6.94	0.004
Face*f	2	0.000762	0.000762	0.000381	7.42	0.003
Face*Rd	2	0.000708	0.000708	0.000354	6.9	0.004
V*f	1	0.000269	0.000269	0.000269	5.24	0.03
V*Rd	1	0.002367	0.002367	0.002367	46.11	0
f*Rd	1	0.00019	0.00019	0.00019	3.71	0.065
Face*V*f	2	0.004162	0.004162	0.002081	40.54	0
Face*V*Rd	2	0.000677	0.000677	0.000338	6.59	0.005
Face*f*Rd	2	0.002267	0.002267	0.001134	22.08	0

R-sq = 92.65%, R-sq (adj) = 87.21%, R-sq(pred) = 76.78%.

Table A3. ANOVA results for Fr.

Source	DF	Seq SS	Adj SS	Adj MS	F-Value	p-Value
Model	11	38,179.4	38,179.4	3470.86	10.61	0
Face	2	2411.9	2411.9	1205.93	3.69	0.035
V	1	946.8	946.8	946.76	2.89	0.098
f	1	7354.6	7354.6	7354.61	22.48	0
Rd	1	3045.6	3045.6	3045.64	9.31	0.004
Face*f	2	2268.3	2268.3	1134.17	3.47	0.042
V*f	1	5432.2	5432.2	5432.17	16.6	0
V*Rd	1	47.1	47.1	47.13	0.14	0.707
f*Rd	1	8125	8125	8125.04	24.83	0
V*f*Rd	1	8547.9	8547.9	8547.91	26.12	0

R-sq = 76.42%, R-sq (adj) = 69.22%, R-sq(pred) = 58.08%.

Table A4. ANOVA results for Ff.

Source	DF	Seq SS	Adj SS	Adj MS	F-Value	p-Value
Model	15	14,204	14,204	946.93	4.58	0
Face	2	556.7	556.7	278.37	1.35	0.274
V	1	5	5	4.98	0.02	0.878
f	1	1944.4	1944.4	1944.39	9.41	0.004
Rd	1	782.8	782.8	782.77	3.79	0.06
Face*V	2	282.6	282.6	141.31	0.68	0.512
Face*f	2	341.6	341.6	170.82	0.83	0.447
V*f	1	1253.6	1253.6	1253.56	6.07	0.019
V*Rd	1	649	649	649.03	3.14	0.086
f*Rd	1	131.7	131.7	131.68	0.64	0.431
Face*V*f	2	1941	1941	970.49	4.7	0.016
V*f*Rd	1	6315.6	6315.6	6315.62	30.56	0

R-sq = 68.23%, R-sq (adj) = 53.34%, R-sq(pred) = 28.52%.

Table A5. ANOVA results for Fa.

Source	DF	Seq SS	Adj SS	Adj MS	F-Value	p-Value
Model	15	43,930.1	43,930.1	2928.7	3.42	0.002
Face	2	860.6	860.6	430.3	0.5	0.61
V	1	4572	4572	4572	5.33	0.028
f	1	4894.9	4894.9	4894.9	5.71	0.023
Rd	1	1578.9	1578.9	1578.9	1.84	0.184
Face*V	2	250	250	125	0.15	0.865
Face*f	2	2738.6	2738.6	1369.3	1.6	0.218
V*f	1	2616.1	2616.1	2616.1	3.05	0.09
V*Rd	1	7079.6	7079.6	7079.6	8.26	0.007
f*Rd	1	2088	2088	2088	2.44	0.128
Face*V*f	2	6908.4	6908.4	3454.2	4.03	0.027
V*f*Rd	1	10,343.1	10,343.1	10,343.1	12.07	0.001

R-sq = 61.56%, R-sq (adj) = 43.54%, R-sq(pred) = 13.51%.

Table A6. The Resulting Sequences of Data Preprocessing.

Run	Sa (μm)	Fr (N)	Ff (N)	Fa (N)
1	0.5734	0.2320	0.2319	0.0503
2	0.3622	0.8267	0.5747	0.5659
3	0.7381	0.9520	0.9092	0.7165
4	0.3580	0.9284	0.5265	0.5305
5	0.8353	0.5039	0.6440	0.7942
6	0.9747	0.7415	0.1827	0.1692
7	0.3749	0.6794	0.4918	0.6898
8	0.5945	0.8936	0.2742	0.2702
9	0.0602	0.6121	0.5255	0.5157
10	0.5987	0.7619	0.6242	0.7043
11	0.6494	0.9908	0.5738	0.1696
12	0.4720	0.5719	0.2908	0.2647
13	0.2270	0.5830	0.5412	0.4074
14	0.7297	0.6879	0.2068	0.3689
15	0.4298	0.5830	0.5412	0.4074
16	0.4636	0.8888	0.4098	0.3967
17	0.6241	0.0551	0.4226	0.1933
18	0.2017	0.6399	0.4768	0.3946
19	0.0285	0.9869	1.0000	0.9941
20	0.1806	0.6054	0.5764	0.4848
21	0.1890	0.5707	0.5443	0.4666
22	0.5396	0.7445	0.6490	0.7096
23	0.5227	0.6530	0.3398	0.6079
24	0.8353	0.5729	0.4826	0.3506
25	0.5861	0.4013	0.1183	0.0394
26	0.2608	0.7938	0.4930	0.5137
27	0.7761	0.8771	0.7718	0.7247
28	0.4593	0.9555	0.5092	0.5218
29	0.8437	0.8615	0.7768	0.9158
30	1.0000	0.8117	0.1519	0.1554
31	0.4129	0.8264	0.6329	0.8664
32	0.7254	0.7250	0.7875	0.7554
33	0.0000	0.3113	0.0000	0.0284
34	0.5016	0.8839	0.5800	0.5131
35	0.7888	0.9706	0.5450	0.4090
36	0.4974	0.6222	0.5271	0.5039
37	0.3622	0.9407	0.8333	0.8969
38	0.7170	0.9659	0.2418	0.4046
39	0.4213	0.6884	0.6724	0.7250
40	0.4551	0.7699	0.8617	0.9193
41	0.6177	0.0000	0.2854	0.0000
42	0.0919	0.6850	0.4778	0.4120
43	0.0665	1.0000	0.9497	1.0000
44	0.1426	0.6260	0.5839	0.4860
45	0.2270	0.6338	0.8926	0.9616
46	0.5269	0.7024	0.5440	0.4997
47	0.5016	0.7820	0.4525	0.7045
48	0.6748	0.9788	0.5848	0.5032

Table A7. Deviation sequences.

Run	Sa (μm)	Fr (N)	Ff (N)	Fa (N)
1	0.4266	0.7680	0.7681	0.9497
2	0.6378	0.1733	0.4253	0.4341
3	0.2619	0.0480	0.0908	0.2835
4	0.6420	0.0716	0.4735	0.4695
5	0.1647	0.4961	0.3560	0.2058
6	0.0253	0.2585	0.8173	0.8308
7	0.6251	0.3206	0.5082	0.3102
8	0.4055	0.1064	0.7258	0.7298
9	0.9398	0.3879	0.4745	0.4843
10	0.4013	0.2381	0.3758	0.2957
11	0.3506	0.0092	0.4262	0.8304
12	0.5280	0.4281	0.7092	0.7353
13	0.7730	0.4170	0.4588	0.5926
14	0.2703	0.3121	0.7932	0.6311
15	0.5702	0.4170	0.4588	0.5926
16	0.5364	0.1112	0.5902	0.6033
17	0.3759	0.9449	0.5774	0.8067
18	0.7983	0.3601	0.5232	0.6054
19	0.9715	0.0131	0.0000	0.0059
20	0.8194	0.3946	0.4236	0.5152
21	0.8110	0.4293	0.4557	0.5334
22	0.4604	0.2555	0.3510	0.2904
23	0.4773	0.3470	0.6602	0.3921
24	0.1647	0.4271	0.5174	0.6494
25	0.4139	0.5987	0.8817	0.9606
26	0.7392	0.2062	0.5070	0.4863
27	0.2239	0.1229	0.2282	0.2753
28	0.5407	0.0445	0.4908	0.4782
29	0.1563	0.1385	0.2232	0.0842
30	0.0000	0.1883	0.8481	0.8446
31	0.5871	0.1736	0.3671	0.1336
32	0.2746	0.2750	0.2125	0.2446
33	1.0000	0.6887	1.0000	0.9716
34	0.4984	0.1161	0.4200	0.4869
35	0.2112	0.0294	0.4550	0.5910
36	0.5026	0.3778	0.4729	0.4961
37	0.6378	0.0593	0.1667	0.1031
38	0.2830	0.0341	0.7582	0.5954
39	0.5787	0.3116	0.3276	0.2750
40	0.5449	0.2301	0.1383	0.0807
41	0.3823	1.0000	0.7146	1.0000
42	0.9081	0.3150	0.5222	0.5880
43	0.9335	0.0000	0.0503	0.0000
44	0.8574	0.3740	0.4161	0.5140
45	0.7730	0.3662	0.1074	0.0384
46	0.4731	0.2976	0.4560	0.5003
47	0.4984	0.2180	0.5475	0.2955
48	0.3252	0.0212	0.4152	0.4968

Table A8. GRC for forty-eight comparability sequences.

Run	Sa (μm)	Fr (N)	Ff (N)	Fa (N)
1	0.5396	0.3943	0.3943	0.3449
2	0.4394	0.7426	0.5404	0.5353
3	0.6563	0.9124	0.8463	0.6382
4	0.4378	0.8748	0.5136	0.5157
5	0.7522	0.5020	0.5841	0.7084
6	0.9518	0.6592	0.3796	0.3757
7	0.4444	0.6093	0.4959	0.6171
8	0.5522	0.8245	0.4079	0.4066
9	0.3473	0.5631	0.5131	0.5080
10	0.5548	0.6774	0.5709	0.6284
11	0.5878	0.9818	0.5399	0.3758
12	0.4864	0.5387	0.4135	0.4047
13	0.3928	0.5453	0.5215	0.4576
14	0.6491	0.6157	0.3866	0.4421
15	0.4672	0.5453	0.5215	0.4576
16	0.4824	0.8181	0.4586	0.4532
17	0.5708	0.3460	0.4641	0.3826
18	0.3851	0.5813	0.4886	0.4523
19	0.3398	0.9745	1.0000	0.9884
20	0.3790	0.5589	0.5413	0.4925
21	0.3814	0.5381	0.5232	0.4838
22	0.5206	0.6618	0.5876	0.6326
23	0.5116	0.5903	0.4309	0.5605
24	0.7522	0.5393	0.4915	0.4350
25	0.5471	0.4551	0.3619	0.3423
26	0.4035	0.7080	0.4965	0.5069
27	0.6907	0.8026	0.6866	0.6449
28	0.4805	0.9183	0.5047	0.5111
29	0.7619	0.7830	0.6913	0.8558
30	1.0000	0.7264	0.3709	0.3719
31	0.4599	0.7423	0.5766	0.7892
32	0.6455	0.6452	0.7017	0.6715
33	0.3333	0.4206	0.3333	0.3398
34	0.5008	0.8115	0.5435	0.5066
35	0.7030	0.9445	0.5236	0.4583
36	0.4987	0.5696	0.5139	0.5020
37	0.4394	0.8940	0.7499	0.8291
38	0.6386	0.9361	0.3974	0.4564
39	0.4635	0.6161	0.6042	0.6452
40	0.4785	0.6848	0.7833	0.8611
41	0.5667	0.3333	0.4117	0.3333
42	0.3551	0.6135	0.4892	0.4595
43	0.3488	1.0000	0.9085	1.0000
44	0.3683	0.5721	0.5458	0.4931
45	0.3928	0.5772	0.8232	0.9286
46	0.5138	0.6269	0.5230	0.4999
47	0.5008	0.6964	0.4773	0.6285
48	0.6059	0.9592	0.5463	0.5016

Table A9. The grey relational grade and its rank.

Run	GRG	Rank
1	0.41828	46
2	0.56443	25
3	0.7633	4
4	0.58548	22
5	0.63666	13
6	0.59156	20
7	0.54167	29
8	0.54778	28
9	0.48285	38
10	0.60786	16
11	0.62134	14
12	0.46084	43
13	0.47928	41
14	0.52336	32
15	0.49788	35
16	0.55309	27
17	0.44089	44
18	0.47686	42
19	0.82568	1
20	0.49293	37
21	0.48161	39
22	0.60066	19
23	0.52333	33
24	0.55448	26
25	0.4266	45
26	0.52873	31
27	0.70624	6
28	0.60364	18
29	0.77301	3
30	0.61729	15
31	0.64201	12
32	0.66599	9
33	0.35677	48
34	0.59059	21
35	0.65736	10
36	0.52104	34
37	0.7281	5
38	0.60712	17
39	0.58224	23
40	0.70195	7
41	0.41126	47
42	0.47932	40
43	0.81433	2
44	0.49482	36
45	0.68045	8
46	0.54089	30
47	0.57576	24
48	0.65326	11

Table A10. Calculation of GRGs main effects.

Parameters	Level 1	Level 2	Level 3	Max-Min
Faces	0.600793	0.56073	0.565408	0.040062
Cutting speed m/min	0.555477	0.59581	-	0.040334
Feed rate (mm/min)	0.543518	0.60777	-	0.064251
Radial depth of cut (mm)	0.586122	0.56517	-	0.020956

References

- Ghio, E.; Cerri, E. Additive Manufacturing of AlSi10Mg and Ti6Al4V Lightweight Alloys via Laser Powder Bed Fusion: A Review of Heat Treatments Effects. *Materials* **2022**, *15*, 2047. [[CrossRef](#)] [[PubMed](#)]
- Torino, P.D.I. Characterization of Powder and Its Bulk Ti-6Al-V Samples Produced by Electron Beam Melting Process. Master's Thesis, Polytechnic University, Bari, Italy, 2019.

3. Murr, L.E.; Quinones, S.A.; Gaytan, S.M.; Lopez, M.I.; Rodela, A.; Martinez, E.Y.; Hernandez, D.H.; Martinez, E.; Medina, F.; Wicker, R.B. Microstructure and Mechanical Behavior of Ti-6Al-4V Produced by Rapid-Layer Manufacturing, for Biomedical Applications. *J. Mech. Behav. Biomed. Mater.* **2009**, *2*, 20–32. [[CrossRef](#)] [[PubMed](#)]
4. Özel, T.; Thepsonthi, T.; Ulatan, D.; Kaftanoglu, B. Experiments and Finite Element Simulations on Micro-Milling of Ti-6Al-4V Alloy with Uncoated and CBN Coated Micro-Tools. *CIRP Ann.-Manuf. Technol.* **2013**, *60*, 85–88. [[CrossRef](#)]
5. Gong, X.; Zeng, D.; Groeneveld-Meijer, W.; Manogharan, G. Additive Manufacturing: A Machine Learning Model of Process-Structure-Property Linkages for Machining Behavior of Ti-6Al-4V. *Mater. Sci. Addit. Manuf.* **2022**, *1*, 6. [[CrossRef](#)]
6. Grierson, D.; Rennie, A.E.W.; Quayle, S.D. Machine Learning for Additive Manufacturing. *Encyclopedia* **2021**, *1*, 576–588. [[CrossRef](#)]
7. Oyelola, O.; Crawforth, P.; M'Saoubi, R.; Clare, A.T. Machining of Additively Manufactured Parts: Implications for Surface Integrity. *Procedia CIRP* **2016**, *45*, 119–122. [[CrossRef](#)]
8. Qin, J.; Hu, F.; Liu, Y.; Witherell, P.; Wang, C.C.L.; Rosen, D.W.; Simpson, T.W.; Lu, Y.; Tang, Q. Research and Application of Machine Learning for Additive Manufacturing. *Addit. Manuf.* **2022**, *52*, 102691. [[CrossRef](#)]
9. Peng, X.; Kong, L.; Fuh, J.Y.H.; Wang, H. A Review of Post-Processing Technologies in Additive Manufacturing. *J. Manuf. Mater. Process.* **2021**, *5*, 38. [[CrossRef](#)]
10. Iquebal, A.S.; Shrestha, S.; Wang, Z.; Manogharan, G.P.; Bukkapatnam, S. Influence of Milling and Non-Traditional Machining on Surface Properties of Ti6Al4V EBM Components. In Proceedings of the 2016 Industrial and Systems Engineering Research Conference, ISERC 2016, Anaheim, CA, USA, 21–24 May 2016; pp. 1120–1125.
11. Gong, X.; Manogharan, G. Machining Behavior and Material Properties in Additive Manufacturing Ti-6Al-4V Parts. In Proceedings of the ASME 2020 15th International Manufacturing Science and Engineering Conference, Online, 3 September 2020; Volume 1. [[CrossRef](#)]
12. Hojati, F.; Daneshi, A.; Soltani, B.; Azarhoushang, B.; Biermann, D. Study on Machinability of Additively Manufactured and Conventional Titanium Alloys in Micro-Milling Process. *Precis. Eng.* **2020**, *62*, 1–9. [[CrossRef](#)]
13. Bonaiti, G.; Parenti, P.; Annoni, M.; Kapoor, S. Micro-Milling Machinability of DED Additive Titanium Ti-6Al-4V. *Procedia Manuf.* **2017**, *10*, 497–509. [[CrossRef](#)]
14. Rysava, Z.; Bruschi, S. Comparison between EBM and DMLS Ti6Al4V Machinability Characteristics under Dry Micro-Milling Conditions. *Mater. Sci. Forum* **2016**, *836–837*, 177–184. [[CrossRef](#)]
15. Çevik, Z.A.; Özsoy, K.; Erçetin, A. The Effect of Machining Processes on the Physical and Surface Morphology of Ti6al4v Specimens Produced through Powder Bed Fusion Additive Manufacturing. *Int. J. 3D Print. Technol. Digit. Ind.* **2021**, *5*, 187–194. [[CrossRef](#)]
16. Yadav, S.P.; Pawade, R.S. Manufacturing Methods Induced Property Variations in Ti6Al4V Using High-Speed Machining and Additive Manufacturing (AM). *Metals* **2023**, *13*, 287. [[CrossRef](#)]
17. Sartori, S.; Moro, L.; Ghiotti, A.; Bruschi, S. On the Tool Wear Mechanisms in Dry and Cryogenic Turning Additive Manufactured Titanium Alloys. *Tribol. Int.* **2017**, *105*, 264–273. [[CrossRef](#)]
18. Anwar, S.; Ahmed, N.; Abdo, B.M.; Pervaiz, S.; Chowdhury, M.A.K.; Alahmari, A.M. Electron Beam Melting of Gamma Titanium Aluminide and Investigating the Effect of EBM Layer Orientation on Milling Performance. *Int. J. Adv. Manuf. Technol.* **2018**, *96*, 3093–3107. [[CrossRef](#)]
19. Dabwan, A.; Anwar, S.; Al-Samhan, A.M.; Nasr, M.M. On the Effect of Electron Beam Melted Ti6Al4V Part Orientations during Milling. *Metals* **2020**, *10*, 1172. [[CrossRef](#)]
20. Dabwan, A.; Anwar, S.; Al-Samhan, A.M.; Alqahtani, K.N.; Nasr, M.M.; Kaid, H.; Ameen, W. CNC Turning of an Additively Manufactured Complex Profile Ti6Al4V Component Considering the Effect of Layer Orientations. *Processes* **2023**, *11*, 1031. [[CrossRef](#)]
21. Dabwan, A.; Anwar, S.; Al-Samhan, A.M.; Nasr, M.M.; AlFaify, A. On the Influence of Heat Treatment in Suppressing the Layer Orientation Effect in Finishing of Electron Beam Melted Ti6Al4V. *Int. J. Adv. Manuf. Technol.* **2022**, *118*, 3035–3048. [[CrossRef](#)]
22. Dabwan, A.; Anwar, S.; Al-Samhan, A.M.; AlFaify, A.; Nasr, M.M. Investigations on the Effect of Layers' Thickness and Orientations in the Machining of Additively Manufactured Stainless Steel 316L. *Materials* **2021**, *14*, 1797. [[CrossRef](#)]
23. Cozzolino, E.; Franchitti, S.; Borrelli, R.; Pirozzi, C.; Astarita, A. Energy Consumption Assessment in Manufacturing Ti6Al4V Electron Beam Melted Parts Post-Processed by Machining. *Int. J. Adv. Manuf. Technol.* **2023**, *125*, 1289–1303. [[CrossRef](#)]
24. Cozzolino, E.; Astarita, A. Energy Saving in Milling of Electron Beam-Melted Ti6Al4V Parts: Influence of Process Parameters. *Int. J. Adv. Manuf. Technol.* **2023**, *127*, 179–194. [[CrossRef](#)]
25. Tran, Q.P.; Nguyen, V.N.; Huang, S.C. Drilling Process on CFRP: Multi-Criteria Decision-Making with Entropy Weight Using Grey-Topsis Method. *Appl. Sci.* **2020**, *10*, 7207. [[CrossRef](#)]
26. Wang, D.; Li, S.; Xie, C. Crashworthiness Optimisation and Lightweight for Front-End Safety Parts of Automobile Body Using a Hybrid Optimisation Method. *Int. J. Crashworthiness* **2021**, *27*, 1193–1204. [[CrossRef](#)]
27. Haq, A.N.; Marimuthu, P.; Jeyapaul, R. Multi Response Optimization of Machining Parameters of Drilling Al/SiC Metal Matrix Composite Using Grey Relational Analysis in the Taguchi Method. *Int. J. Adv. Manuf. Technol.* **2008**, *37*, 250–255. [[CrossRef](#)]
28. Dabwan, A.; Ragab, A.E.; Saleh, M.A.; Ghaleb, A.M.; Ramadan, M.Z.; Mian, S.H.; Khalaf, T.M. Multiobjective Optimization of Process Variables in Single-Point Incremental Forming Using Grey Relational Analysis Coupled with Entropy Weights. *Proc. Inst. Mech. Eng. Part L J. Mater. Des. Appl.* **2021**, *235*, 2056–2070. [[CrossRef](#)]

29. Yu-Lai, S.; Wen-Tao, Z.; Guoling, L.; Yuan, T.; Shan, T. Optimal Design of Large Mode Area All-Solid-Fiber Using a Gray Relational Optimization Technique. *Optik* **2021**, *242*, 167188. [[CrossRef](#)]
30. Chen, H.; Lu, C.; Liu, Z.; Shen, C.; Sun, M. Multi-Response Optimisation of Automotive Door Using Grey Relational Analysis with Entropy Weights. *Materials* **2022**, *15*, 5339. [[CrossRef](#)]
31. Ameen, W.; Al-Ahmari, A.; Mohammed, M.K. Self-Supporting Overhang Structures Produced by Additive Manufacturing through Electron Beam Melting. *Int. J. Adv. Manuf. Technol.* **2019**, *104*, 2215–2232. [[CrossRef](#)]
32. Umer, U.; Ameen, W.; Abidi, M.H.; Moiduddin, K.; Alkhalefah, H.; Alkahtani, M.; Al-Ahmari, A. Modeling the Effect of Different Support Structures in Electron Beam Melting of Titanium Alloy Using Finite Element Models. *Metals* **2019**, *9*, 806. [[CrossRef](#)]
33. Ameen, W.; Al-Ahmari, A.; Mohammed, M.K.; Abdulhameed, O.; Umer, U.; Moiduddin, K. Design, Finite Element Analysis (FEA), and Fabrication of Custom Titanium Alloy Cranial Implant Using Electron Beam Melting Additive Manufacturing. *Adv. Prod. Eng. Manag.* **2018**, *13*, 267–278. [[CrossRef](#)]
34. Biffi, C.A.; Fiocchi, J.; Ferrario, E.; Fornaci, A.; Riccio, M.; Romeo, M.; Tuissi, A. Effects of the Scanning Strategy on the Microstructure and Mechanical Properties of a TiAl6V4 Alloy Produced by Electron Beam Additive Manufacturing. *Int. J. Adv. Manuf. Technol.* **2020**, *107*, 4913–4924. [[CrossRef](#)]
35. Sun, J.; Guo, Y.B. A Comprehensive Experimental Study on Surface Integrity by End Milling Ti-6Al-4V. *J. Mater. Process. Technol.* **2009**, *209*, 4036–4042. [[CrossRef](#)]
36. Liu, H.; Wu, C.H.; Chen, R.D. *Effects of Cutting Parameters on the Surface Roughness of Ti6Al4V Titanium Alloys in Side Milling*; Trans Tech Publications, Ltd.: Zurich, Switzerland, 2011.
37. Oosthuizen, G.A.; Nunco, K.; Conradie, P.J.T.; Dimitrov, D.M. The Effect of Cutting Parameters on Surface Integrity in Milling Ti6Al4V. *S. Afr. J. Ind. Eng.* **2016**, *27*, 115–123. [[CrossRef](#)]
38. Rao, R.; Yadava, V. Multi-Objective Optimization of Nd:YAG Laser Cutting of Thin Superalloy Sheet Using Grey Relational Analysis with Entropy Measurement. *Opt. Laser Technol.* **2009**, *41*, 922–930. [[CrossRef](#)]
39. Wei, G. Grey Relational Analysis Model for Dynamic Hybrid Multiple Attribute Decision Making. *Knowl.-Based Syst.* **2011**, *24*, 672–679. [[CrossRef](#)]
40. Ertuğrul, İ.; Öztaş, T.; Özçil, A.; Öztaş, G. Grey Relational Analysis Approach in Academic Performance Comparison of University a Case Study of Turkish Universities. *Eur. Sci. J.* **2016**, *12*, 1857–7881.
41. Shah, A.; Azmi, A.; Khalil, A. Grey Relational Analyses for Multi-Objective Optimization of Turning S45C Carbon Steel. In *IOP Conference Series: Materials Science and Engineering, Proceedings of the 2nd International Manufacturing Engineering Conference and 3rd Asia-Pacific Conference on Manufacturing Systems (iMEC-APCOMS 2015), Kuala Lumpur, Malaysia, 12–14 November 2015*; IOP Publishing: Bristol, UK, 2023.
42. Soorya Prakash, K.; Gopal, P.M.; Karthik, S. Multi-Objective Optimization Using Taguchi Based Grey Relational Analysis in Turning of Rock Dust Reinforced Aluminum MMC. *Measurement* **2020**, *157*, 107664. [[CrossRef](#)]
43. Lotfi, F.H.; Fallahnejad, R. Imprecise Shannon's Entropy and Multi Attribute Decision Making. *Entropy* **2010**, *12*, 53–62. [[CrossRef](#)]
44. Li, X.; Wang, K.; Liu, L.; Xin, J.; Yang, H.; Gao, C. Application of the Entropy Weight and TOPSIS Method in Safety Evaluation of Coal Mines. *Procedia Eng.* **2011**, *26*, 2085–2091. [[CrossRef](#)]
45. Dabwan, A.; Anwar, S.; Al-samhan, A. Effects of Milling Process Parameters on Cutting Forces and Surface Roughness When Finishing Ti6al4v Produced by Electron Beam Melting. *Int. J. Mech. Mater. Eng.* **2020**, *14*, 324–328.
46. Liu, S.; Lin, Y. Introduction to Grey Systems Theory. In *Understanding Complex Systems*; Springer: Berlin/Heidelberg, Germany, 2010; Volume 68, pp. 1–399. [[CrossRef](#)]

Disclaimer/Publisher's Note: The statements, opinions and data contained in all publications are solely those of the individual author(s) and contributor(s) and not of MDPI and/or the editor(s). MDPI and/or the editor(s) disclaim responsibility for any injury to people or property resulting from any ideas, methods, instructions or products referred to in the content.